Characterizing Mist Distribution in Through-Tool Minimum Quantity Lubrication Drills

Jay K. Raval
Department of Mechanical Engineering,
Texas A&M University,
College Station, TX 77840
e-mail: jkraval@tamu.edu

Yi-Tang Kao
Department of Mechanical Engineering,
Texas A&M University,
College Station, TX 77840
e-mail: yitangkao@tamu.edu

Bruce L. Tai
Department of Mechanical Engineering,
Texas A&M University,
College Station, TX 77840
e-mail: btai@tamu.edu

The mist distribution is a critical factor in through-tool minimum quantity lubrication (MQL) drilling since a small amount of lubricant is used. However, it has rarely been discussed because of the difficulty in measuring the mist flow experimentally. In this paper, an optical approach is developed to approximate the mist distribution by using high-speed images from multiple angles. Drill bits with two through-tool channel shapes (circle and triangle) and three helix angles (0 deg, 30 deg, and 45 deg) are 3D printed for mist distribution analysis. Furthermore, computational fluid dynamics (CFD) is conducted to investigate the underlying physics behind mist flow variations. The results show that, in the circular channel, the mist is concentrated near the periphery; the low concentration region shifts away from the chisel point as the helix angle increases. For the triangular channel, the mist is concentrated near three vertices but is less affected by the helix angle. Furthermore, based on the CFD solution, high mist concentration tends to be in low-velocity regions and vice versa. This study confirms a noticeable difference of mist flow distribution in different through-tool channel designs. [DOI: 10.1115/1.4045799]

Keywords: MQL, drilling, flow characterization, optical tomography, CFD, machining processes, modeling and simulation

1 Introduction

Minimum quantity lubrication (MQL) is a method of cutting fluid application in machining processes. In MQL, a small quantity of lubricant is delivered to the cutting zone by atomizing it using pressurized air to provide lubrication and cooling during the machining process. Studies have found that MQL, if properly applied, can reduce the machining costs by up to 20% due to the absence of filtration and recirculation systems for coolant and the lower flow rates of the lubricant [1,2]. Therefore, MQL has been widely adopted in the industry. Commercial MQL systems can be classified either as a single-channel or a dual-channel system. In a single-channel MQL system, the aerosol is generated first and then transferred through the machine tool to the cutting zone. While in a dual-channel system, the lubricant and the pressurized air are transferred separately and atomized near the cutting zone. Dual-channel systems are more effective because of the mist consistency at the outlet and faster response time during tool change [3,4]. MQL can also be applied either externally or internally. In an externally applied MQL, the nozzle is pointed toward the cutting zone, while in an internally applied MQL system, the through-tool channels are used to deliver the air-lubricant mist. For operations like drilling, internally applied MQL is required because of direct access to the cutting zone [5].

Flow parameters in MQL, regardless of the configuration, are known to influence the tool life, surface finish, and material removal rate [6–12]. Researchers have found that the nozzle position and orientation, inlet pressure, and lubricant affect the quality of machining [13,14]. It has been concluded that keeping the nozzle close to the cutting zone provides the best cutting performance [15–17]. Another study reported that droplet diameter should be small enough to increase the surface area to volume ratio but not so small that the lubricant droplets cannot be carried along with the air [18]. It can be summarized from these studies that, when dealing with extremely low quantity of lubricant to achieve the optimal performance, proper control over the mist flow is important and necessary. Studies have also been conducted for mist characteristics such as droplet diameter, droplet speed, and flow rate [18–21]. Experimental and computational works have been carried out to characterize the flow [22–24]. Tool manufacturers have used these results to design and optimize through-tool channels for MQL drilling tools, but no published data are available to verify if the channel shape and size are the reasons for the improvement. Because commercial drill bits also differ in other design parameters, all these parameters have compounded effects on the flow during drilling. This leads to a need for fundamentally understanding the mist distribution in the through-tool channels and the associated effect on lubricant coverage on the cutting edges. Moreover, the heat generation and tool wear on the cutting edge are not uniform. Therefore, whenever a low quantity of lubricant is used, the targeted delivery of the lubricant is important. With the understanding of how the flow distributes in the through-tool channels, the distribution of flow on the cutting edge can be correlated and better tools can be designed. This design methodology can improve the cutting performance.

MQL is a multiphase flow, and multiple methods are available for multiphase flow measurement. These methods can be broadly classified by invasive and noninvasive methods. Invasive methods are not applicable for the through-tool channels because insertion of the sensor can disrupt the flow pattern in a small channel (1–2 mm) leading to inaccurate measurements. There have been advancements in the field of noninvasive measurement and flow visualization techniques, such as X-ray transmission tomography, X-ray radiography, X-ray diffraction tomography, optical tomography, laser Doppler anemometry, particle image velocimetry, phase Doppler anemometry, and fluorescence particle image velocimetry [25]. For a fast fluid motion like MQL (typically over 100 m/s) [8], all the X-ray-based methods are incapable because they are time consuming and cannot be used on moving objects. Other planar measurement techniques like laser Doppler anemometry and particle image velocimetry are inefficient for extremely turbulent flow in MQL [26]. There can be out-of-plane motion of droplets, which produces data loss between consecutive images and makes image correlation not reliable. Therefore, instead of adopting an existing method, this study proposes an optical approach using multiple high-speed images to determine the flow distribution.

Manuscript received July 17, 2019; final manuscript received December 10, 2019; published online December 20, 2019. Assoc. Editor: Laine Mears.

In the optical method, a high-speed camera is used to instantaneously visualize flow distribution. The image acquisition is performed from multiple angles. Since the flow is translucent, the obtained image is a 2D projection of 3D flow distribution. The measurements from multiple angles are used to decouple the 2D images and reconstruct a 3D flow distribution. However, this research is limited to approximation only because a complete reconstruction (e.g., optical tomography) requires an extremely steady flow and nearly no light attenuation, which are not seen in a typical MQL system. In addition to the mist distribution measurement, a computational fluid dynamics (CFD) simulation is also carried out to correlate the mist distribution and air flow pattern and velocity as a function of drill helix angle and the through-tool channel geometry.

To structure this paper, Section 1 deals with the background and the introduction of the MQL process and flow measurement techniques. Section 2 explains the experimental setup, materials, and the optical method used in this study. Section 3 provides the results obtained using the experimental procedure. Section 4 provides the numerical results followed by comparison with the experimental results. Section 5 and 6 present discussion and conclusions, respectively.

2 Materials and Methods

2.1 Experimental Setup. A lab scale setup was developed to mimic the flow in an actual drilling process as shown in Fig. 1. The setup consisted of a dual-channel MQL system developed by UNIST (Grand Rapids, MI), a rotary union, an atomizing chamber, a drill bit, two light sources, and a high-speed camera. The dual-channel MQL system allowed control of the lubricant flow rate, while the air pressure is controlled by the pressure valve. The rotary union was used to allow rotation of the shaft without rotating the tubes. An atomizing chamber was kept before the drill bit, where the lubricant is atomized into mist by the pressurized air and then delivered to the cutting zone through the coolant channels in the tool. High-speed imaging was carried out using a Phantom MiroLab 310 camera developed by Vision Research (Wayne, NJ) to capture the flow distribution. The camera has a capacity of capturing 3200 frames/s (fps) grayscale images at 1280×800 resolution. For this experiment, the frame rate was kept at 1000 fps and a resolution of 512×512. The effect of drill rotation was neglected because the flow velocity in the axial direction is in the order of 100 m/s and the channels are only about 2.5 mm away from the axis of the drill. Therefore, the centrifugal force generated due to the rotation of drill have minimum effect unless at high rotational speeds (more than 10,000 rpm) [27].

A commercially available MQL fluid, Coolube 2210 (UNIST, Grand Rapids, MI) was used as the lubricant. It has an intermediate value of viscosity and surface tension among all the available MQL fluids in the market [28]. The lubricant flow rate ranges from 5 ml/h to 100 ml/h in actual MQL applications, and so the lubricant flow rate was kept constant at 40 ml/h for all the experiments. This allowed the flow to be in a practically used range and also easy enough to be observed using the optical method. For a controlled experiment, stereolithography printing was used (Form 2, Formlabs, Somerville, MA) to manufacture the drill bits provided its high-dimensional accuracy and surface finish. Clear resin purchased from Formlabs was used as the drill material. This allowed the drills be to be transparent. The use of 3D printing to manufacture drills allowed the variation of a single-design parameter without changing other values. To ensure that the printed polymer can represent a tungsten carbide (WC) surface, the contact angle with the lubricant was measured and found to be 15 deg to 18 deg, which fell in a comparable range for WC [29]. The surface roughness inside the through-tool channels was also measured with a cut-off length of 80 μm, and the roughness value (Ra) for carbide tools was found to be 0.205 μm and that for 3D printed drill was found to be 0.805 μm. Since both the values were in the submicron level and the contact angles were also in the same range, it can be assumed that the interaction between the lubricant and the 3D printed tool is similar to that between the lubricant and WC tool. It should be noted that, for this study, the effect of interior surface roughness of the channels was not particularly considered.

2.2 Design of Experiments. The design of drill bits was based on commonly available drills in the market. Helix angle and channel shape were selected as the two variables. Two channel shapes, circular and triangular, and three helix angles, 0 deg, 30 deg, and 45 deg, were used to develop a 2-by-3 full factorial design of experiments, as shown in Fig. 2(*a*). These channel shapes and helix angles are the standard shapes and the values used for off the shelf drilling tools available in the market [30]. Furthermore, an extended study was conducted to analyze the effect of channel orientation on mist distribution, in which the triangular channel shape was rotated by 180 deg and named as the reversed triangle. To avoid any effect of channel length on the mist distribution, the channel length for all the drill bits was kept constant by altering the drill length, as shown in Fig. 2(*b*). For a 10-mm diameter MQL drill available in market, the channel diameter was measured as 1.6 mm. Therefore, the circular channel has a diameter of 1.6 mm, and the triangular channels have a side length of 2.15 mm. This was done to keep the channel cross-sectional area the same for all the cases to ensure the same volumetric flow rate. Also, the pitch circle diameter of the through-tool channels for all the cases was 4.5 mm based on the commercial tool. For the imaging purpose, the flow was allowed through only one coolant channel, while the other channel was blocked to avoid overlay of mist flow patterns.

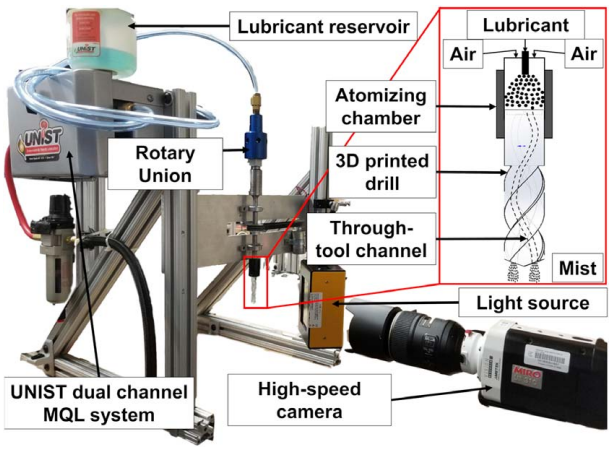

Fig. 1 Experimental setup to simulate flow distribution in MQL drilling

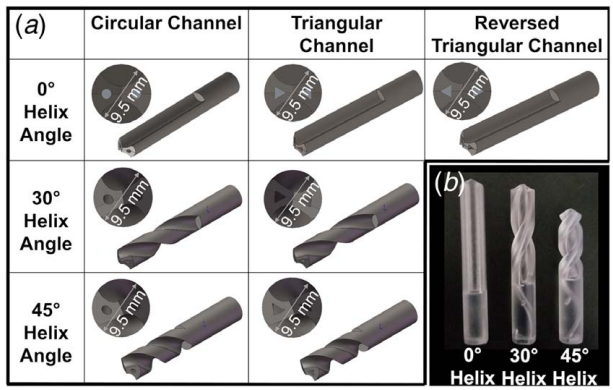

Fig. 2 (*a*) Design of experiments and (*b*) change in the length of the drill with respect to the helix angle to keep the through-tool channel lengths constant

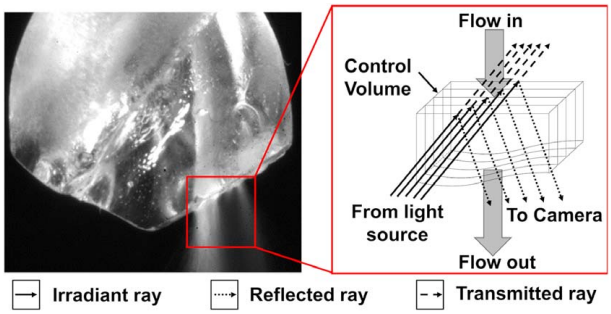

Fig. 3 Camera capturing a 2D superposition of 3D flow on planes at different depths

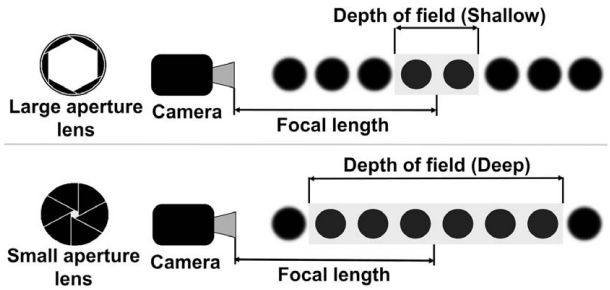

Fig. 4 Effect of aperture on the depth of field at the same focal length

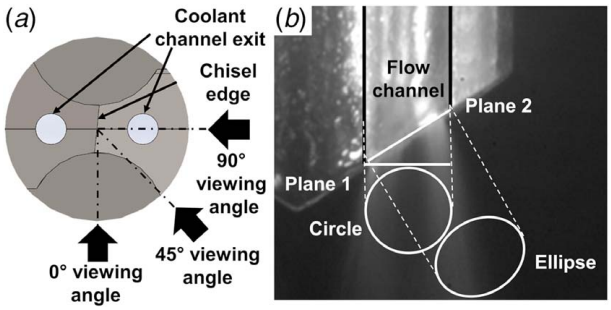

Fig. 5 (*a*) Viewing angles for analyzing the flow as seen from the bottom of the drill and (*b*) selection of the cross-sectional plane for analysis (an image of 0 deg view angle)

2.3 Image Acquisition Method. For the multiphase flow in MQL, the primary phase is air and the secondary phase is lubricant. The air is transparent and does not reflect any light; only the liquid droplets will reflect the light. This reflected light can be used as a signal to predict the mist distribution. The higher the mist concentration, the higher the amount of reflected light. The size of the coolant channel is of the order of 1–2 mm, and thus, it can be assumed that there is no attenuation of light intensity across the channel diameter.

The image captured is a 2D overlay of the flow in 3D; therefore, the image captured by the camera can be seen as a superposition of mist distribution on an infinite number of planes as shown in Fig. 3. To get a clear image, it is important to set the camera parameters in such a manner that the whole control volume is in focus. Therefore, the aperture of the camera was kept at f/32 to increase the depth of field. The decrease in aperture increased the depth of field and allowed the camera to focus on a deeper region; however, this also reduced the amount of light entering the camera. This is explained schematically in Fig. 4. Therefore, the exposure time was increased to provide more time for light to enter the camera. It was not necessary to get a clear image of droplets since no image correlation was conducted to define the velocity field. Instead, a streak line pattern created by droplet paths under long exposure is ideal to estimate the mist distribution. With such a setting, the flow distribution can be accurately captured. As shown in Fig. 3, higher mist concentration seen near the chisel edge of the drill reflects more light compared with the other portion. Therefore, the intensity of the pixel in the image captured is directly proportional to the mist density along a line passing through the pixel and perpendicular to the camera sensor.

In this study, three viewing angles, 0 deg, 45 deg, and 90 deg, were selected to approximately predict the mist distribution. Multiple angles are needed to understand the 3D flow distribution from 2D images. The viewing angles are named based on the angle of rotation of the drill on its axis, as shown in Fig. 5(*a*). Figure 5(*b*) shows an actual image from the circular channel drill. As shown, the flow can be either analyzed in plane 1 or plane 2. Plane 1 is the plane perpendicular to the axis of the tool, while plane 2 is the plane parallel to the exit area of the tool. For this study, the flow was analyzed on plane 2 because the mist distribution there depicts the mist distribution at the exit of the channel, which, in reality, contacts the workpiece.

2.4 Image Analysis Procedure. Figure 6 shows three measurements in an identical flow condition but under different light irradiances (denoted as level 1 to level 3) to demonstrate the image processing method and the effects of irradiance. To obtain the mist distribution profile, the intensities of pixels were plotted along the direction x_1 (which is parallel to plane 2 in Fig. 5(*b*)). The intensity represents the mist density. With an 8-bit greyscale camera, the intensity value ranges from 0 to 255, with 255 being the brightest. To reduce the effect of ambient light, experiments were conducted in a dark room. However, the background cannot be tuned down to completely dark, and the remaining intensity value is termed as noise. Since the lighting conditions and testing environment are the same during a particular experiment, the value of noise is constant throughout the experiment and thus can be subtracted from each data point, as shown in Fig. 7(*a*).

As shown, irradiance is a key factor to be considered to ensure that images are comparable. For the same flow condition, a higher irradiance results in brighter pixels. This effect can be removed if all the profiles are scaled to a 0 to 1 arbitrary unit. Figure 7(*b*) shows scaled profiles of three images captured for the same flow condition (Fig. 6) after the constant noise is removed. The raw profiles do not align with each other, but once they are scaled (Fig. 7(*b*)), they show a fairly consistent trend. This indicates that the mist distribution measurement is independent of the irradiance. Nonetheless, no direct conclusion can be made about mist concentration from the scaled profiles unless the effect of channel

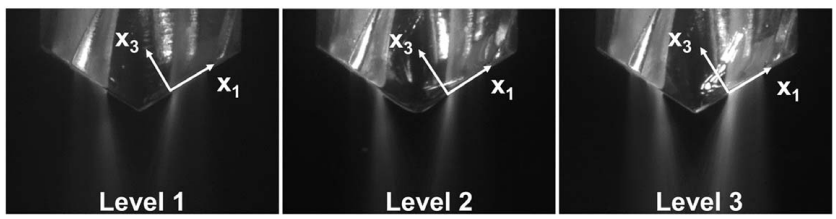

Fig. 6 Image acquired at different intensity levels

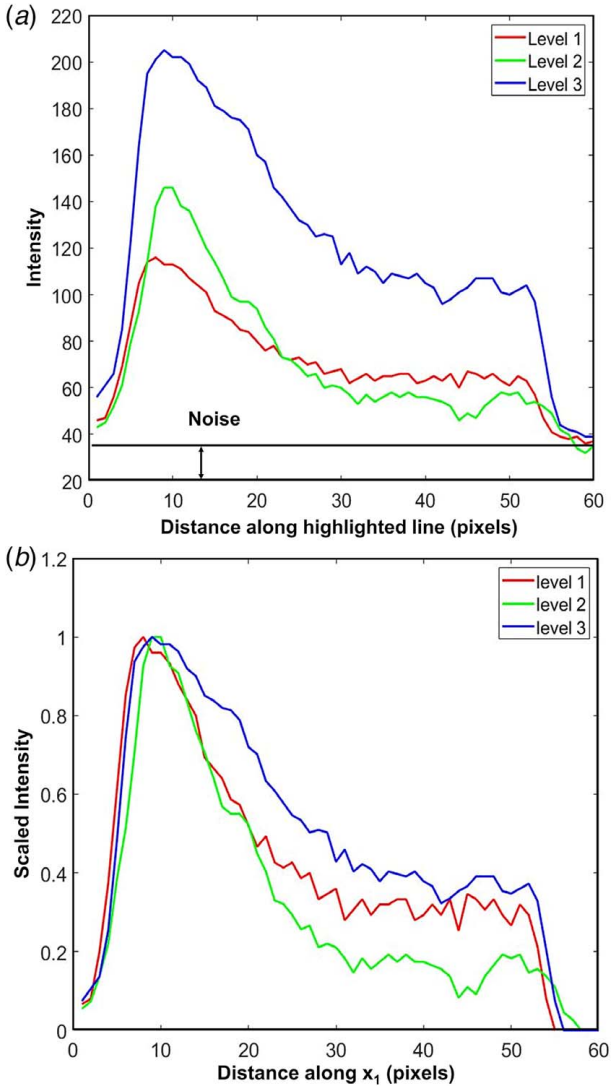

Fig. 7 (*a*) Raw intensity plot for all the levels of intensity and (*b*) scaled intensity plot for all the levels of intensity

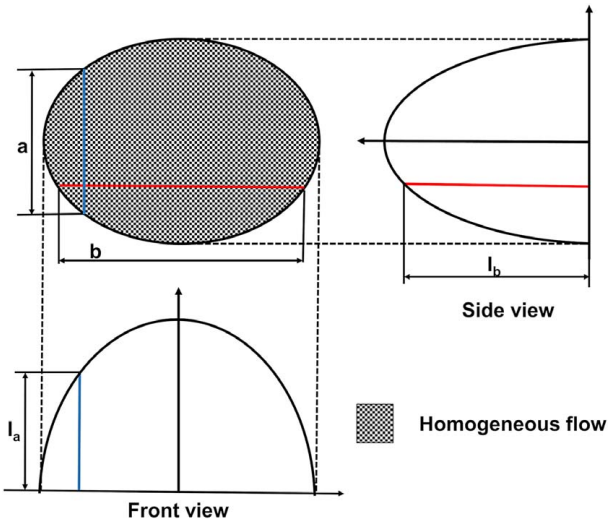

Fig. 8 Ideal flow profiles in 0 deg and 90 deg viewing angles assuming homogeneous flow

shape is taken into account. For example, for a homogeneously distributed mist (homogeneous flow) across a circular channel with an elliptical cross-sectional area, the projected 2D intensity plot, measured from the camera image, would be a superimposed intensity along the viewing direction, as shown in Fig. 8, where the intensity value of I_a and I_b are proportional to the depth of a and b, respectively. In other words, despite a homogeneous flow, the image will show more concentration at the center of the x_1-axis.

Figure 9 summarizes a step-by-step procedure for image processing using a circular channel with a 0 deg helix angle at 0 deg viewing angle as an example. Figure 9(*a*) shows a sample image acquired using the image acquisition method. The intensity profiles are plotted along the x_1 direction. To ensure repeatability, five measurements under the same flow condition were used to obtain an averaged plot, as shown in Fig. 9(*b*). Then, the noise is subtracted to obtain a filtered profile, and the profile is scaled to 0–1 (Fig. 9(*c*)). To remove the shape effect, the ideal profile from a homogeneous flow is generated based on the channel geometry, as shown in Fig. 9(*d*). The ideal profile should be scaled to have the same area under the curve as that shown in Fig. 9(*c*) to represent an equal mist flow rate. Finally, the ideal profile is subtracted from the experimental profile to obtain a normalized profile (Fig. 9(*e*)). The total area under the curve must be zero as a result of the equal mist flow rate. With the normalized profile, the positive regions represent the high mist flow rate in the depth direction of the x_1-axis. Similarly, the negative regions represent a low mist flow rate. Note that the definition of the high or low mist flow rate is relative to a homogenous flow.

The normalization process described in Fig. 9 is repeated for three viewing angles for a given case to generate an approximation of 3D flow distribution. The probable high mist concentration regions can be mapped by back projection from each viewing angle to the channel cross-section, as shown in Fig. 10. The shaded area indicates a high probability of high mist concentration.

3 Experimental Results

This section presents the results obtained for each case shown in the design of experiments (Fig. 2). Figure 11 shows the probable high mist concentration regions obtained using the image acquisition and analysis method explained in Sec. 2. For all the results, the chisel edge of the drill is always on the left side of the exit area.

The result of the 0 deg helix angle circular channel shows a probable high mist concentration zone near the periphery of the channel. The low mist concentration region is found to be in the center of the channel. The result is nearly axis symmetric, and thus, an annular type of flow is observed, where the secondary phase (lubricant) flows near the periphery of the channel, and the primary phase (air) flows in the center of the channel. It should be noted that a low mist concentration zone does not mean the absence of secondary phase; it only means low mist concentration compared with a homogenous mist concentration.

For the 30 deg helix angle circular channel, the exit area is an ellipse rotated by about 30 deg. The low mist concentration zone shifts toward the right, i.e., away from the chisel edge of the drill bit. This creates a wider high mist concentration zone near the chisel edge of the drill and a narrower high mist concentration zone toward the drill margin. Similarly, for the 45 deg helix angle circular channel, the low mist concentration region shifts farther away from the chisel edge of the drill, and the exit area is an ellipse rotated by about 45 deg.

For the 0 deg helix angle triangular channel, the result shows probable high mist concentration in the vertices of the channel and low mist concentration in the center of the channel. For the 30 deg helix angle triangular channel, unlike the circular channel, the low mist concentration zone shifts slightly downward. For the 45 deg helix angle triangular channel, the high mist concentration still remains at the vertices, but the low mist concentration zone shifts slightly upward compared with the 30 deg helix angle

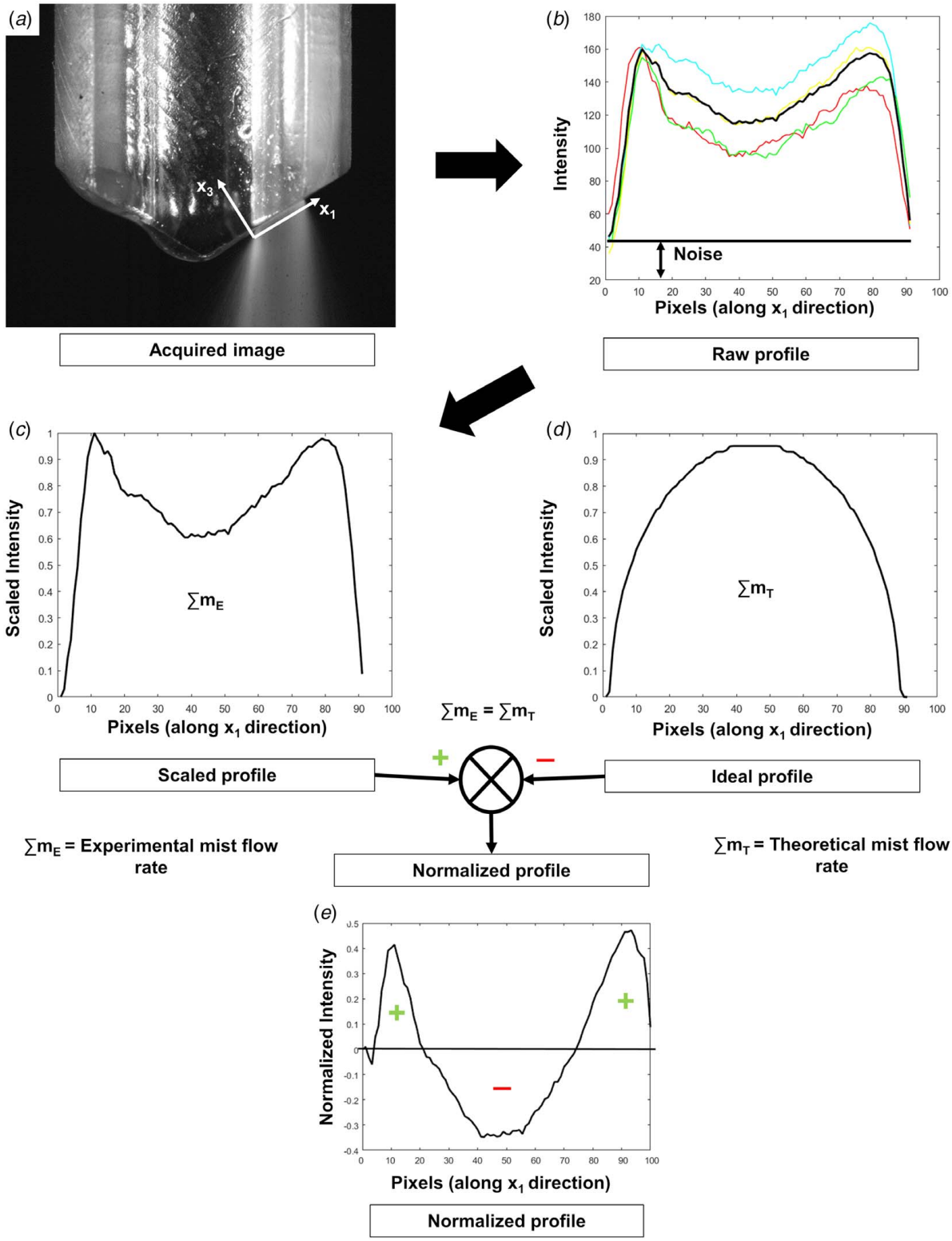

Fig. 9 Step-by-step procedure for image analysis using an example of 0 deg helix angle circular channel at 0 deg viewing angle: (*a*) sample image, (*b*) raw profile plotted along highlighted line, (c) scaled profile plotted along x_1-axis, (*d*) ideal profile from a homogeneous flow, and (e) normalized profile along x_1-axis

triangular channel. The result of the 0 deg helix angle reversed triangular channel is almost a mirror image of the result for the 0 deg helix angle triangular channel. This result is interesting because as the channel was rotated by 180 deg, the mist distribution was also rotated by 180 deg. This means that the mist distribution is dependent on the channel orientation.

4 Numerical Results and Comparison

This section discusses about the numerical method used to generate the flow velocity contours at the exit of the through-tool channel. These results are compared with the experimental results to find any correlation.

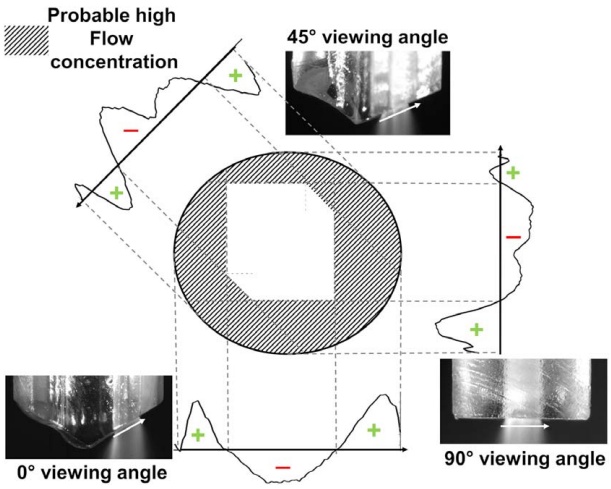

Fig. 10 Flow concentration mapping using normalized profiles from three viewing angles

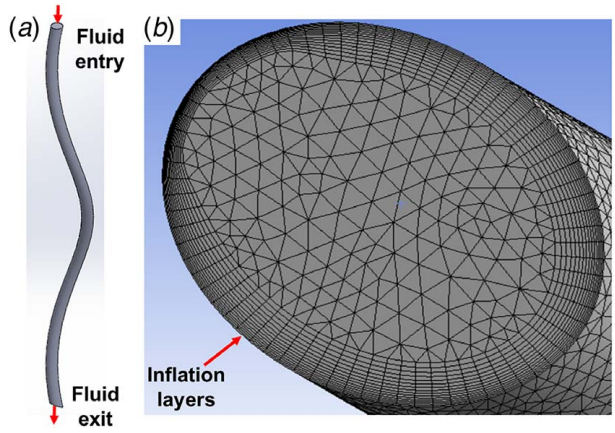

Fig. 12 (*a*) Control volume for numerical solution and (*b*) cross-sectional mesh for numerical solution

4.1 Setup and Boundary Conditions. Technically, a multiphase model is required to obtain an accurate solution for MQL. However, the droplet size in MQL is typically less than 10 μm [26], and the channel size is usually of the order of millimeters in diameter and tens of millimeters in length. Therefore, to accurately track the movement of droplets through the control volume, the mesh size must be smaller than 1 μm at all locations. Because of this requirement of extremely small mesh size for a comparatively large control volume, the multiphase flow simulation is extremely time and power consuming. Therefore, it was hypothesized that since most of the flow in MQL is air (more than 99.99% in volume and 99% in weight), a single-phase simulation can be carried out to obtain the flow field identical or similar to the exact multiphase flow. Figure 12 shows a model example of the circular channel and cross-sectional mesh for the single-phase flow simulation. The simulation was conducted using ANSYS-FLUENT version 16.2.

Inflation was used to generate a mesh, which is finer near the boundary and larger in the center region to catch the boundary layer while reducing the computation time. For boundary conditions, the inlet boundary condition was kept as constant velocity with a magnitude of 300 m/s for all the cases. This particular number was provided by Ford Motor Company for a 1- to 2-mm channel measured using the jet impingement method [31]. The exit boundary condition was kept as constant pressure of 0 bar gauge pressure since the channels are exiting in the atmosphere. Flow velocity of 300 m/s results in the Mach number of 0.87, and this means that the change in the density of the fluid is nonnegligible. Thus, a density-based solver was used for the numerical solution. The Reynolds number calculated for the flow is 48,000, which makes the flow completely turbulent. This matches with the published data available about MQL. Therefore, the κ-ϵ model, a two-equation turbulence model, was used to simulate the flow [32].

4.2 Comparison of Experimental and Numerical Results. Figure 13 shows the numerical results obtained for each case shown in the design of experiments. The result for the 0 deg helix angle circular channel is essentially a pipe flow, where the high flow velocity region is at the center of the channel, and the velocity reduces as moved toward the edge of the channel. The result of the 30 deg helix angle circular channel shows a shift in the high flow velocity region toward the right of the channel and away from the chisel edge of the drill. This happens because of the centrifugal forces generated due to the helical motion of the fluid. The results were verified with the results obtained by Yamamoto et al. [33]. The velocity contours obtained by the CFD solution matched with the velocity contours obtained by Yamamoto et al. For the

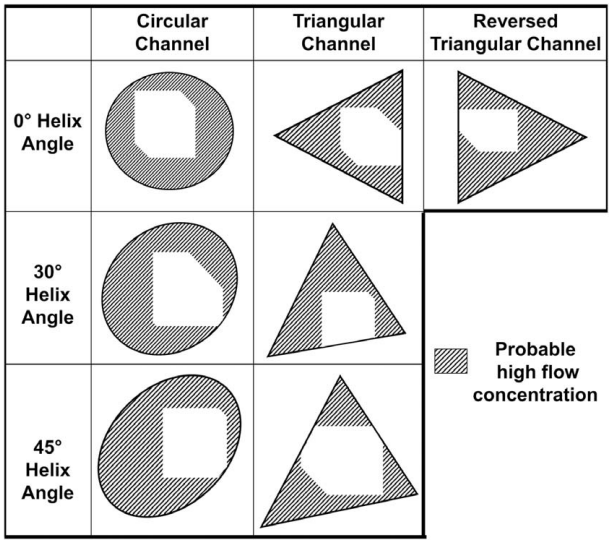

Fig. 11 Experimentally obtained probable high flow concentration zones

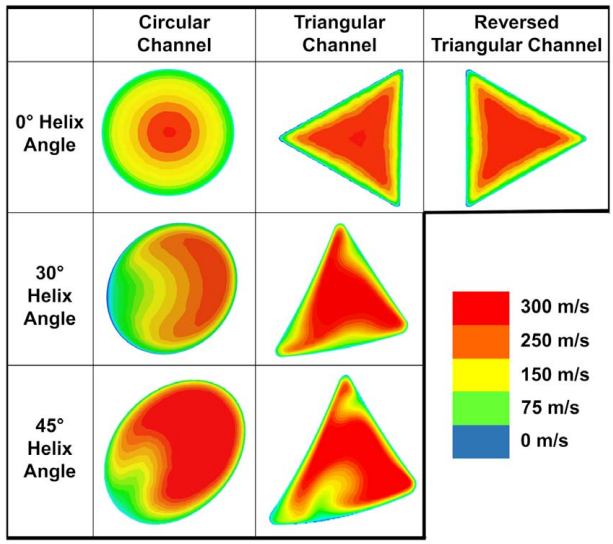

Fig. 13 CFD solutions for all tested cases

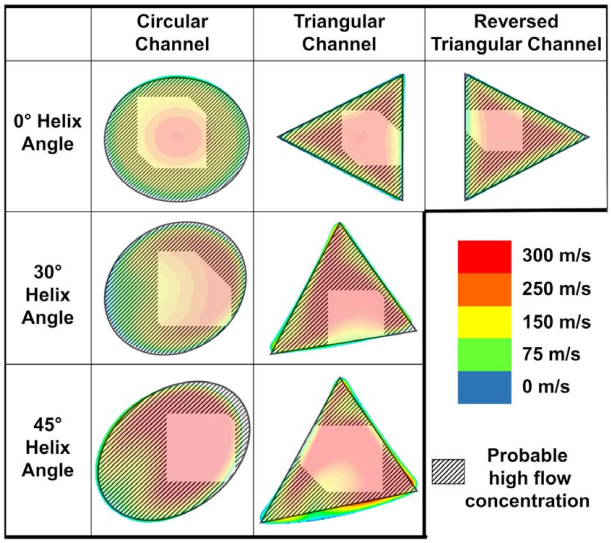

Fig. 14 Overlaid images of experimental and numerical results

45 deg helix angle circular channel, the result shows a similar trend as the 30 deg helix angle channel; however, the shift of the high-velocity region is more severe compared to that of the previous case.

For the 0 deg helix angle triangular channel, the exit velocity contours show the high-velocity region in the center of the channel, while the low-velocity region is in proximity of the channel periphery. In the case of the 30 deg helix angle channel, the high flow velocity region remains in the center of the channel, but the flow contours twist across the center of the channel. This happens because of the flow along a helical path. The twisting of the flow contours increases as the helix angle is increased. The case of the 45 deg helix angle channel shows a more twisted flow pattern. However, twisting of the flow is not observed on the measurement results (Fig. 11) due to the limited resolution of the flow mapping method. For the 0 deg helix angle reversed triangular channel, the exit velocity contours are almost a mirror image of the exit velocity contours of 0 deg helix angle triangular channel. This verifies a nearly mirror distribution in Fig. 11 between these cases.

Figure 14 compares the experimentally obtained probable high mist concentration zone and numerically obtained velocity contours at the exit of the channel. Both the results are overlaid for comparison purposes. These results clearly show a strong correlation between the velocity and flow distribution in multiphase flows like MQL. For each of the case, the probable high flow concentration region is either directly over the low flow velocity region or in its proximity and vice versa. Therefore, single-phase velocity contours can be used to predict the mist distribution in the multiphase flow with an acceptable accuracy level.

5 Discussion

After comparing the experimental and numerical results, it is evident that the mist concentration is higher in the low-velocity region, and thus, the oil droplets tend to gather in the low-velocity regions. This means the mist distribution is a function of velocity. This type of flow can also be explained by the substantial difference in the volumetric flow rate between the air and oil phases (100 L/min versus 1 mL/min), which falls in the annular flow regime. Any physical process always occurs in such a manner that the amount of energy lost during the process is minimum. Therefore, less viscous air goes into the high-velocity (low flow resistance) region and forces the more viscous lubricant into the low-velocity region [34]. Another possible explanation for the distribution is using the adhesion force. The contact angles for lubricant and drill material are small, which means the surface energy of the tool is higher than that of the lubricant, and therefore, the adhesion forces pull the droplets from the center of the channel to the periphery of the channel. Because of which, high mist concentration is obtained near the periphery of the channel. The mist distribution obtained can be a result of either of these phenomena or a combination of these. Further investigation is required to make any conclusions about the governing phenomena. This study was limited to the flow distribution at the exit of through-tool channels in MQL drills. During the cutting process, the presence of the workpiece also influences the flow distribution, and the actual distribution of the flow on the cutting edge may change.

There are certain limitations of the current flow measurement technique that needs to be dealt with. First, the mist flow rate fluctuates due to the positive displacement pump used in the MQL machine. The frequency of the pump was set to 50 strokes per minute, and this nonsteady-state flow may slightly change the flow distribution during a pulse cycle. Second, it was assumed that there is no attenuation of light as it travels through the control volume. The incorporation of light attenuation is difficult because the attenuation is a function of the flow density, and the flow density is unknown unless the data are available about the attenuation. Therefore, an iterative method like algebraic reconstruction technique can be used to first generate preliminary results and then refine the results based on the previous results [35]. For this study, only a qualitative comparison was carried out between the mist distribution and the velocity distribution. To obtain a more quantitative mist distribution, tomography techniques in computed tomography and magnetic resonance imaging can be applied with more viewing angles. However, these tomography techniques also require fully defined attenuation and ideally a steady flow to reconstruct the 3D image correctly.

6 Conclusions

The current study analyzed the mist distribution in drills employing MQL and investigated the effect of channel shape, channel orientation, and helix angle using the amount of light reflected from the flow as a signal for mist density. Three different helix angles and three different channel shapes were analyzed for their effect on mist distribution. The mist distribution changed as the channel shape and helix angle were changed; therefore, it can be concluded that the channel shape, the orientation, and the helix angle all have an effect on the mist distribution obtained. Based on the CFD results, it was found that the velocity distribution in the channel is one of the major factors affecting the mist distribution. The high-velocity regions tend to have low mist concentration, whereas the low-velocity regions tend to have high mist concentration. Although the effects on the machining performance of such variations are still unclear, this study shows the evidence of differences in flow distribution to support the continuous investigation of a machining study.

Acknowledgment

The authors would like to thank National Science Foundation (NSF) for providing funding to the project (Grant No. 1760985). Dr. David Stephenson from Ford Motor Company (Livonia, MI) to provide the velocity measurement data. Mr. Tim Walker from UNIST (Grand Rapids, MI) for providing the UNIST Coolubricator dual-channel MQL system and Coolube 2210 lubricant used for this study.

References

[1] Tai, B. L., Stephenson, D. A., Furness, R. J., and Shih, A. J., 2014, "Minimum Quantity Lubrication (MQL) in Automotive Powertrain Machining," Procedia CIRP, **14**(6th CIRP International Conference on High Performance Cutting, HPC2014), pp. 523–528.

[2] Furness, R., Stoll, A., Nordstrom, G., Martini, G., Johnson, J., Loch, T., and Klosinski, R., 2006, "Minimum Quantity Lubrication (MQL) Machining for Complex Powertrain Components," Proceedings of the ASME 2006

International Manufacturing Science and Engineering Conference. Manufacturing Science and Engineering, Parts A and B., Ypsilanti, Michigan, Oct. 8–11.
[3] Stephenson, D. A., and Agapiou, J. S., 2016, *Metal Cutting Theory and Practice*, CRC Press, Boca Raton, FL.
[4] Stephenson, D. A., Hughey, E., and Hasham, A. A., 2019, "Air Flow and Chip Removal in Minimum Quantity Lubrication Drilling," Procedia Manufacturing, **34**, pp. 335–342.
[5] Aoyama, T., Kakinuma, Y., Yamashita, M., and Aoki, M., 2008, "Development of a New Lean Lubrication System for Near Dry Machining Process," CIRP Ann., **57**(1), pp. 125–128.
[6] Filipovic, A., and Stephenson, D. A., 2006, "Minimum Quantity Lubrication (MQL) Applications in Automotive Power-Train Machining," Mach. Sci. Technol., **10**(1), pp. 3–22.
[7] Heinemann, R., Hinduja, S., Barrow, G., and Petuelli, G., 2006, "Effect of MQL on the tool life of small twist drills in deep-hole drilling," J. Mach. Tools Manuf., **46**(1), pp. 1–6.
[8] Lerma, I., Jimenez, M., Edinbarough, I., Krell, J., and Hung, N. P., 2015, "Characterization of Micromist for Effective Minimum Quantity Lubrication," Adv. Mater. Res., **1115**, pp. 43–46.
[9] Tai, B. L., Jessop, A. J., Stephenson, D. A., and Shih, A. J., 2012, "Workpiece Thermal Distortion in Minimum Quantity Lubrication Deep Hole Drilling—Finite Element Modeling and Experimental Validation," ASME J. Manuf. Sci. Eng., **134**(1), p. 011008.
[10] Tasdelen, B., Wikblom, T., and Ekered, S., 2008, "Studies on Minimum Quantity Lubrication (MQL) and Air Cooling at Drilling," J. Mater. Process. Technol., **200**(1), pp. 339–346.
[11] Vivek, T. G., Vikas, T. P., Kuppan, P., Balan, A. S. S., and Oyyaravelu, R., 2016, "Experimental Investigation of Machining Parameter Under MQL Milling of SS304," IOP Conf. Ser. Mater. Sci. Eng., **149**(1), p. 012023.
[12] Dhar, N. R., Kamruzzaman, M., and Ahmed, M., 2006, "Effect of Minimum Quantity Lubrication (MQL) on Tool Wear and Surface Roughness in Turning AISI-4340 Steel," J. Mater. Process. Technol., **172**(2), pp. 299–304.
[13] Sharma, A. K., Tiwari, A. K., and Dixit, A. R., 2016, "Effects of Minimum Quantity Lubrication (MQL) in Machining Processes Using Conventional and Nanofluid Based Cutting Fluids: A Comprehensive Review," J. Cleaner Prod., **127**, pp. 1–18.
[14] Zhu, G., Yuan, S., and Chen, B., 2019, "Numerical and Experimental Optimizations of Nozzle Distance in Minimum Quantity Lubrication (MQL) Milling Process," Int. J. Adv. Manuf. Technol., **101**(1), pp. 565–578.
[15] Masoudi, S., Vafadar, A., Hadad, M., and Jafarian, F., 2018, "Experimental Investigation Into the Effects of Nozzle Position, Workpiece Hardness, and Tool Type in MQL Turning of AISI 1045 Steel," Mater. Manufac. Process., **33**(9), pp. 1011–1019.
[16] López de Lacalle, L. N., Angulo, C., Lamikiz, A., and Sánchez, J. A., 2006, "Experimental and Numerical Investigation of the Effect of Spray Cutting Fluids in High Speed Milling," J. Mater. Process. Technol., **172**(1), pp. 11–15.
[17] Ueda, T., Hosokawa, A., and Yamada, K., 2005, "Effect of Oil Mist on Tool Temperature in Cutting," ASME J. Manuf. Sci. Eng., **128**(1), pp. 130–135.
[18] Park, K.-H., Olortegui-Yume, J., Yoon, M.-C., and Kwon, P. J. I. J. O. M. T., 2010, "A Study on Droplets and Their Distribution for Minimum Quantity Lubrication (MQL)," Int. J. Mach. Tools Manuf., **50**(9), pp. 824–833.
[19] Husted, B. P., Petersson, P., Lund, I., and Holmstedt, G., 2009, "Comparison of PIV and PDA Droplet Velocity Measurement Techniques on Two High-Pressure Water Mist Nozzles," Fire Safety J., **44**(8), pp. 1030–1045.
[20] Rahim, E. A., and Dorairaju, H., 2018, "Evaluation of Mist Flow Characteristic and Performance in Minimum Quantity Lubrication (MQL) Machining," Measurement, **123**, pp. 213–225.
[21] Sovani, S. D., Chou, E., Sojka, P. E., Gore, J. P., Eckerle, W. A., and Crofts, J. D., 2001, "High Pressure Effervescent Atomization: Effect of Ambient Pressure on Spray Cone Angle," Fuel, **80**(3), pp. 427–435.
[22] Chen, Z., Atmadi, A., Stephenson, D. A., Liang, S. Y., and Patri, K. V., 2000, "Analysis of Cutting Fluid Aerosol Generation for Environmentally Responsible Machining," CIRP Ann., **49**(1), pp. 53–56.
[23] Dasch, J., and Kurgin, S., 2010, "A Characterisation of Mist Generated From Minimum Quantity Lubrication (MQL) Compared to Wet Machining," Inter. J. Mach. Machin. Mater., **7**(1), pp. 82–95.
[24] Duchosal, A., Leroy, R., Vecellio, L., Louste, C., and Ranganathan, N., 2013, "An Experimental Investigation on Oil Mist Characterization Used in MQL Milling Process," Int. J. Adv. Manuf. Technol., **66**(5), pp. 1003–1014.
[25] Falcone, G., Hewitt, G., and Alimonti, C., 2009, *Multiphase Flow Metering: Principles and Applications*, Elsevier, New York.
[26] Khan, W. A., Hoang, N. M., Tai, B., and Hung, W. N. P., 2018, "Through-Tool Minimum Quantity Lubrication and Effect on Machinability," J. Manuf. Proc., **34**(B), pp. 750–757.
[27] Hewson, A. S. J., Merson, R., Summers, J. E., and Thompson, H., 2014, "Internal Twist Drill Coolant Channel Modelling Using Computational Fluid Dynamics," In: Oñate, E, Oliver, J and Huerta, A, (eds.) Proceedings, vol. II. 11th World Congress on Computational Mechanics (WCCM), 5th European Conference on Computational Mechanics (ECCM), 6th European Conference on Computational Fluid Dynamics (ECFD), Barcelona, Spain, July 20–25.
[28] Tai, B. L., Dasch, J. M., and Shih, A. J., 2011, "Evaluation and Comparison of Lubricant Properties in Minimum Quantity Lubrication Machining," Mach. Sci. Technol., **15**(4), pp. 376–391.
[29] Li, Q., Lerma, I., Alvarado, J., Edinbarough, I., and Hung, W. N. P., 2015, "Characterization of Micromist for Effective Machining," ASME 2015 International Mechanical Engineering Congress and Exposition,Houston, TX, Nov. 13–19, p. V02AT02A058.
[30] Tai, B., Stephenson, D., Furness, R., and Shih, A., 2017, Minimum Quantity Lubrication for Sustainable Machining.
[31] Stephenson, D. A., Hughey, E., and Hasham, A., 2019, "Air Flow and Chip Removal in Minimum Quantity Lubrication Drilling," Procedia Manufacturing, **34**(47th SME North American Manufacturing Research Conference, NAMRC 47, PA), pp. 335–342.
[32] Rohit, J. N., Surendra Kumar, K., Sura Reddy, N., Kuppan, P., and Balan, A. S. S., *Computational Fluid Dynamics Analysis of MQL Spray Parameters and Its Influence on MQL Milling of SS304*, Springer, Singapore, pp. 45–78.
[33] Yamamoto, K., Alam, M. M., Yasuhara, J., and Aribowo, A., 2000, "Flow Through a Rotating Helical Pipe With Circular Cross-Section," Int. J. Heat Fluid Flow, **21**(2), pp. 213–220.
[34] Schwarzkopf, J. D., Sommerfeld, M., Crowe, C. T., and Tsuji, Y., 2011, *Multiphase Flows With Droplets and Particles*, CRC Press, Boca Raton, FL.
[35] Gordon, R., Bender, R., and Herman, G. T., 1970, "Algebraic Reconstruction Techniques (ART) for Three-Dimensional Electron Microscopy and X-Ray Photography," J. Theor. Biol., **29**(3), pp. 471–481.